15TH IEA HEAT PUMP CONFERENCE
MAY 26–29, 2026 | HOFBURG
VIENNA 2026
DECARBONISATION THROUGH INNOVATION

Insights into a Field Test of a Predictively Controlled Air-Source Heat Pump in Single-Family Homes using non-linear optimization

David Schmitt[a,b,*], Lucas Müller[a], Tobias Reum[a,b], Fabian Ochs[b], Tobias Schrag[a]

[a] Institute of new Energy Systems, Technische Hochschule Ingolstadt, Esplanade 10, 85049 Ingolstadt, Germany
[b] Department of Structural Engineering and Material Sciences, University of Innsbruck, Technikerstr. 13, A-6020 Innsbruck, Austria

Abstract

Heat pumps are a key technology for decarbonizing residential heating, with air-source heat pumps being the most common choice in German single-family homes. However, their efficiency decreases during winter when heating demand is highest. Predictive control approaches such as Model Predictive Control (MPC) can mitigate this limitation by shifting operation to periods with more favourable ambient conditions while maintaining thermal comfort. This paper presents the design, implementation, and field evaluation of a predictively controlled air-source heat pump system that utilizes the building mass as thermal storage. The controller was tested in a single-family house equipped with ceiling heating, concrete core activation, and a thermal buffer storage. Simplified models were developed to ensure computational feasibility. A hierarchical control structure combining long-term (7 days) and short-term (16 hours) MPC was implemented. First evaluations of the field measurements show an improvement of 4-27% in the heat pump performance factor by shifting operation to higher ambient temperatures. However, the use of building thermal mass led to increased total electrical consumption, highlighting the drawback of thermal activation and the need for careful implementation of such control algorithms. Future work will extend the evaluation to a full heating season and further refine the controller design.

© HPC2026.
Selection and/or peer-review under the responsibility of the organizers of the 15th IEA Heat Pump Conference 2026.

Keywords: model predictive control, air-source heat pump, thermal building mass activation, field testing

1. Introduction

Heat Pumps are a key technology for decarbonizing the domestic heating sector, as they enable the efficient use of renewable energy sources for space heating and domestic hot water production. In the German single family-home (SFH) segment the air-source heat pump (ASHP) is the most installed kind of heat pump due to easy installation and low investment costs. Due to low outdoor temperatures, ASHPs suffer from low efficiencies in winter while the heat demand is the highest. However, fluctuations in the outdoor temperature, e.g. day-to-night differences, offer the potential to improve the efficiency of ASHPs by shifting the operation.

Predictive control algorithms such as Model Predictive Control (MPC) take changing boundary conditions into account, such as weather predictions, dynamic electricity prices and PV-generation to schedule an optimized ASHP operation. Using MPC with ASHPs yields the potential to improve the efficiency of such domestic heating systems and results in reduced operational costs, lower energy demand and consequently a lower need for an extensive expansion of renewable energies.

For a flexible ASHP operation energy storage is needed. A larger storage capacity leads to greater flexibility, thereby increasing the optimization potential achievable with MPC. Using the building mass as energy storage offers a large storage capacity which can be activated at low temperature levels. The latter is additionally advantageous for the efficiency of heat pumps, which is higher at low sink temperatures.

* Corresponding author. *E-mail address:* david.schmitt@thi.de

Thür et al. investigated the potential of using building mass as a thermal energy storage to increase the amount of directly consumed electric energy provided by a rooftop PV-system, also called self-consumption, in an SFH. In this simulative study, different ways of activating the building mass were compared. As a result of activating the building mass with a floor heating system and a simple rule-based control logic, the self-consumption rate was doubled while the operational costs could be reduced by 30% in comparison to a conventional controller. [1]

A similar setup was investigated in a simulative study by Kuboth et al. using an MPC to control the heating system of an SFH. The authors show that the operational costs are reduced by 12% while the self-consumption rate increased by only 4%. This shows the high sensitivity of the results on the boundary conditions such as weather conditions and building parameters. In the study it was shown that the MPC increased the user comfort through the prevention of thermal comfort limit violations in comparison to a conventional controller. Simultaneously the seasonal performance factor of the ASHP increased by 3%. [2]

When designing an MPC for real operation, several challenges must be tackled. First, simplified modelling approaches must be found which offer a short computation time while representing all relevant details. Several studies analyzed different modelling approaches of ASHPs and buildings and their impact on the MPC performance. Verhelst et al. showed that the frequency dependency of modulating ASHP's efficiency has a significant impact on the result of the optimized operation schedule and thus should be considered [3]. In terms of the building model, Magni et al. compared different simplified approaches to represent the building dynamics and calculate the heat demand [4]. The authors give insights into which simplification can reduce computational time, and which details are necessary to ensure model accuracy. A second challenge is the definition of a reasonable prediction horizon. The prediction horizon describes the length of the future period for which the schedule is calculated by the MPC. As stated in the review by Hilliard et al., the commonly used prediction horizon for building systems is 24 hours to capture day-night effects for operation shifting [5]. However, when the building mass is utilized as a storage medium, a longer prediction horizon may be advantageous due to its inert thermal behaviour. As demonstrated by D'Ettorre et al., an optimal design is achieved when the prediction horizon is aligned with the time constant of the controlled system [6]. An increase in the prediction horizon results in exponentially higher computational effort, which may prevent real-time MPC operation. Hierarchical setups offer a solution to tackle this challenge [7].

In this contribution the design and implementation of a hierarchical MPC to optimize the operation of an ASHP using building mass as storage capacity is introduced. The developed MPC addresses the challenges from literature mentioned before and offers a methodology for the application of such advanced control algorithms. First, the demonstration building including the monitoring system is described. Second, simplified models are derived and integrated into a hierarchical MPC framework. Third, SFH was monitored over two heating seasons using a conventional controller and the developed MPC. An initial comparison of both operations is given, and preliminary conclusions from the field test are drawn.

2. Description of the Demonstration Building

The SFH serving as demonstration building is located in South Germany. It was built in 2019 and has a net floor space of 260 m². The building envelope is well-insulated which is represented by the low specific annual space heating demand of 22.6 kWh/(m²a). The building consists of 11 heated rooms distributed on ground and first level and an unheated basement.

The hydraulic installation of the heating system is shown in Fig. 1 schematically. Space heating (SH) and domestic hot water (DHW) are both provided by an ASHP and distributed via an 800-l thermal buffer storage (TBS). The upper part of the TBS is connected to a freshwater station for DHW purposes. The lower part of the TBS is connected to a distribution unit from which the heat is distributed to the rooms.

Each room can be heated in two ways: ceiling heating (CH) and concrete core activation (CCA). A schematic cross-section including the thickness of each layer according to the planning documentation of the demonstration building is shown in Fig. 2. The CH pipes are placed close to the surface to quickly heat up the room. The CCA pipes are placed in the center of the concrete which leads to a slower response in the room temperature. Additional insulation elements have been installed between CH and CCA pipes resulting in a mixed layer of insulation and concrete. The driving idea for this system is that the CH can be directly coupled with the CCA pipes. This offers the possibility to actively discharge the upper concrete layer using the CCA pipes and to operate the upper concrete layer as thermal storage.

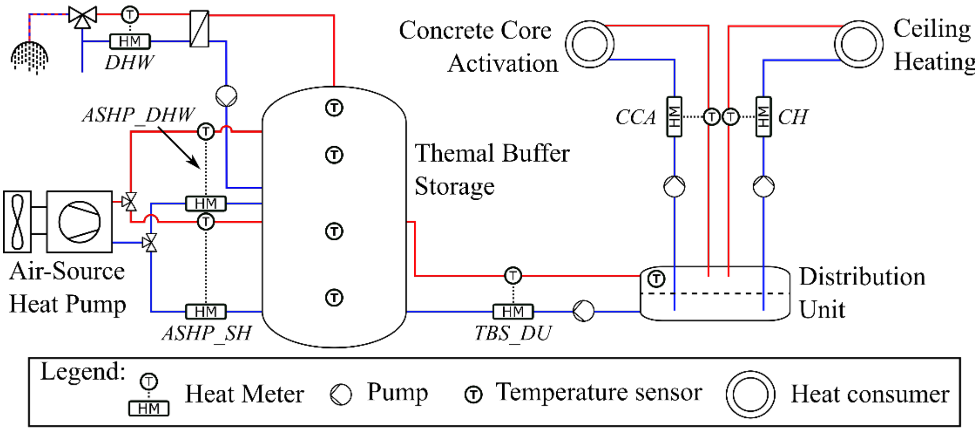

Figure 1. Schematic hydraulic interconnection of the building's heating system including the naming convention of the heat meters

The benefits of this operation mode and its additional flexibility potential have been analyzed by validated simulations [8]. Even though the system is installed in the demonstration building, the CCA pipes are not used for active discharging. Thus, active discharge is not considered further in this study.

The dynamic behavior of the demonstration building has been investigated in a simulation study [9]. The authors conclude that when the CCA pipes are used, the building keeps the indoor temperatures for around 3 days before it drops below 20 °C during winter. This information is important when designing a predictive controller as inert systems require longer prediction horizons, see section 3.3. In the following, the upper concrete layer and the mixed layer combined are referred to as the thermally activated building system (TABS), see Fig. 2. The lower concrete layer will be referred to as CH.

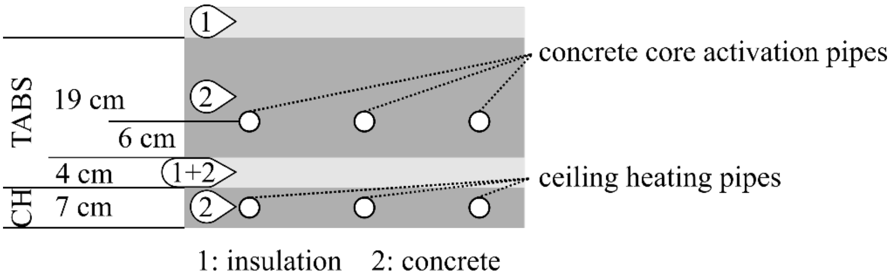

Figure 2. Schematic cross section of the ceiling element

To monitor the building's behavior and evaluate the efficiency of the energy system, several heat meters were installed in the demonstration building, see Fig. 1. On the supply side, two heat meters *ASHP_SH*, and *ASHP_DHW* were installed between ASHP and TBS to measure the supplied heat for SH and DHW purposes respectively. DHW consumption is measured by the heat meter *DHW* behind the freshwater station. The SH demand is measured by the two heat meters *CCA,* and *CH* to monitor the corresponding thermal energy used to activate the two layers of the ceiling. Additionally, the heat meter *TBS_DU* measures the heat transferred from the TBS to the distribution unit to quantify the distribution losses individually. Heat meters of type *Multical 603* and *Multical 403* of the manufacturer *kamstrup* were installed to measure the heat supply and demand. The measurements by the heat meters are stored every five minutes in a database server. According to the information in the data sheet, the uncertainties of the measured energy are at 3%. Electricity metes were installed to measure the heat pumps electricity consumption, having a measurement uncertainty of 2%.

The indoor conditions such as room air temperature, CO_2, and volatile organic compounds (VOC) of each room are measured by sensors of type *Multisensor true presence* from the manufacturer *Steinel* mounted on each room's ceiling. Since there is no information about the temperature sensor types inside the devices, the measurement uncertainty was estimated to be around 0.5 K, which represents a typical value for digital sensors.

During the construction process of the building, temperature sensors were placed inside the ceiling's concrete of each room. According to the information provided by the homeowner, Pt500 sensors were installed at the center of each room at the same depth as the CCA pipes 6 cm above the mixed layer, see Fig. 2. Each sensor was put into a plastic pipe; thus the sensor is not in direct contact with the concrete. The plastic pipe wall and the air inside the pipe introduces an uncertainty to the measured value. The influence on the measured value is hard to quantify due to unknown geometrical and material properties of the plastic pipe, unknown volume of trapped air between sensor and pipe wall, and possible natural convection processes within the pipe. For the uncertainty induced by the sensor installation a constant value of 5% was assumed. The accuracy classification of the Pt500 sensors was unknown, thus the accuracy class B was assumed. This resulted in a total uncertainty of 7% within the range of 20-40°C. The variation of the sensor placement was assumed to be smaller than 0.5 cm as the plastic pipe was fixed on the same frame as the CCA pipes were placed.

The measurement uncertainties are summarized in Table 1.

Table 1. Measurement uncertainties of the installed measurement devices

Measurement Device	Uncertainty
Heat meter	3%
Electricity mete	2%
Indoor temperature	±0.5 K
TABS temperature	7%
TABS sensor placement	±0.5 cm

3. Development and Implementation of the Model Predictive Controller

For the energy systems of the demonstration building an MPC was designed to optimally control the ASHP based on outdoor temperatures. Drgoňa et al. give a good overview of the basics, and different ways of how an MPC can be designed and implemented [10]. First, a model is developed which represents dynamic system behavior. Second, an optimization problem based on an objective function and boundary conditions is defined. Third, the MPC is implemented in a so-called rolling horizon principle, which means that the MPC is executed iteratively, and the calculated schedule is updated regularly. The rolling horizon principle helps to reach robust control of the system as prediction errors can be compensated by updating the schedule according to the new system states. The MPC was designed and implemented using the *MATLAB Model Predictive Control Toolbox* [11].

3.1. Prediction model of the building energy system

The prediction model has to be both as accurate as necessary to minimize the prediction error, and as simple as possible to minimize the computational time. This is especially critical in a rolling-horizon setup, since the MPC runs continuously and the optimization problem must be solved between successive executions. This is discussed in section 3.3 where the implementation is described in detail. To represent the building energy system three sub models were defined: ASHP, TBS, and building.

3.1.1. Model of the Air-Source Heat Pump

The ASHP model follows a black box model approach. Polynomial equations were fitted based on measurement data to represent the electric consumption and heating power at different operation points. The information was taken from the manufacturer's datasheet which follows the standard measurements according to EN 14511, in which the operation conditions and measurement durations are regulated [12]. The resulting measurements represent the steady state behavior of the ASHP at a certain source and sink temperature, and, in case of a modulating ASHP, the inverter frequency.

For the installed ASHP only the data sheet was available, which includes a broad range of source and sink temperatures at maximal heating power. The heating and electric power according to the information in the data sheet is shown in Fig. 3.

The heating power increases approximately linearly and levels off at source temperatures above −5 °C. This behavior is attributed to an internal control strategy that limits the maximum inverter frequency at higher source temperatures. This assumption is supported by the observation that the electrical power remains nearly constant at source temperatures below −5 °C and above 10 °C, while a pronounced decrease occurs in the intermediate range. Since the internal control logic is not accessible, this fact cannot be confirmed. In real operation this is no limitation of the ASHP functionality since the building's heat demand at higher source temperatures is lower so it can be fully covered also with lower inverter frequencies.

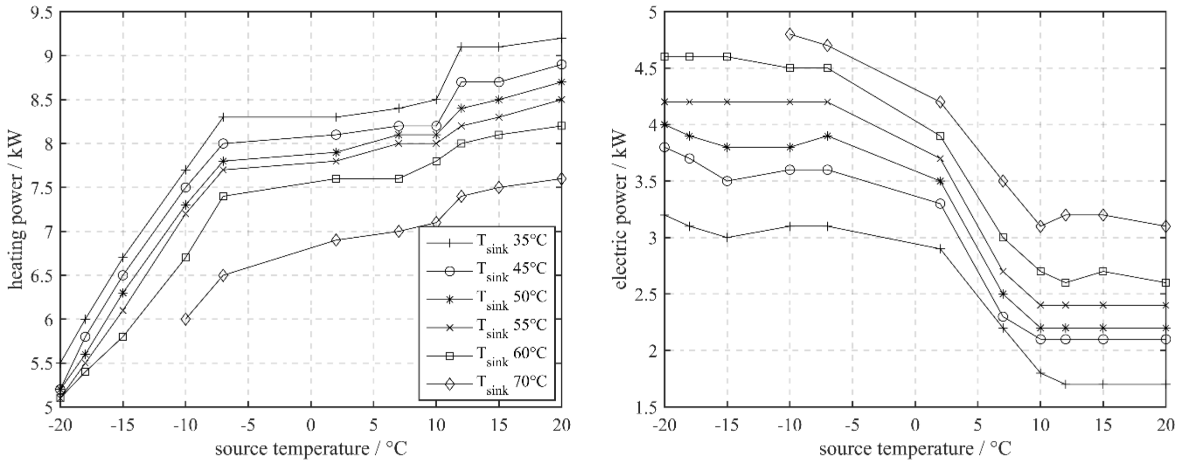

Figure 3. Manufacturer data sheet of the air-source heat pump left: heating power, right: electric power

The performance data provided in the datasheet were represented using a polynomial model. Heating and electrical power (P) were expressed as functions of the source temperature (T_{so}), sink temperature (T_{si}), and a modulation factor (f_{mod}), as shown in Eq. (1). For heating power, polynomial orders of n=m=4 were selected, while for electrical power n=3 and m=1 were used. The model parameters were identified using the MATLAB Curve Fitting Toolbox [13], yielding root mean squared errors of 147.5 W and 184.5 W for heating and electrical power, respectively.

$$P(T_{so}, T_{si}) = \sum_{j=0}^{n} \sum_{i=0}^{m} \left(p_{ij} \cdot T_{so}^{j} \cdot T_{si}^{i}\right) \cdot f_{mod} \tag{1}$$

The derived polynomial models include the assumption of a linear part load behavior. Based on the studies of Verhelst et al. in case of a linear part load behavior, the cost function must be adopted to penalize higher modulation [3]. The suggested approach was used for the given MPC, which is described in section 3.2.

3.1.2. Model of the thermal buffer storage

A commonly adopted approach in the literature for modelling a thermal storage within an MPC framework is the one-dimensional model using lumped thermal masses [2,6], often referred to as resistor–capacitor (RC)-models. In this approach, the temperature distribution of the storage is represented along its height while assuming radial homogeneity. The thermal buffer storage is discretized into multiple thermal nodes, each defined by a uniform temperature, a heat capacity, and parameters accounting for heat and mass transfer. The TBS of the demonstration building was modelled using two thermal nodes. The number of nodes was chosen since the TBS provides thermal energy at two different temperature levels, one for DHW (T_{DHW}) and one for SH (T_{SH}) purposes, see Fig. 4.

The temperature change of each thermal node was modelled based on the corresponding energy balance including heat losses to the basement, and charging and discharging heat fluxes. The heat losses are calculated based on the temperature difference between the node and a constant basement temperature (T_{base}) of 18 °C, using a constant heat loss coefficient of 1 W/K. The heat loss coefficient was calculated based on the storage geometry and insulation information of the installed TBS in the demonstration building.

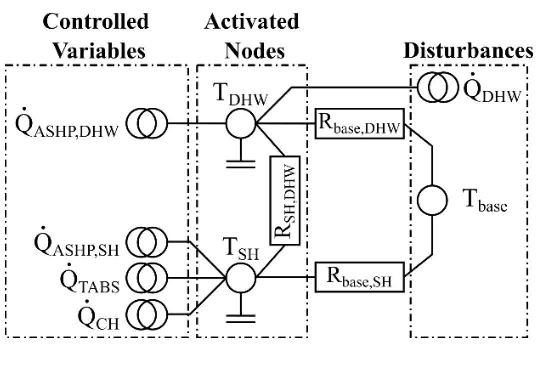

Figure 4. RC-model of the thermal buffer storage

It is assumed that heat is transferred between the thermal nodes only through conduction, while mixing and convection are neglected. A constant heat conduction factor of 2 W/K was used, which was fit using measurement data of the real TBS. Due to this assumption the model is only valid for $T_{SH} \leq T_{DHW}$, which was implemented as a constraint in the formulation of the optimization problem, see section 3.2.

The DHW demand is modelled as a load profile based on measurement data. One year of measurement data was used to derive consumption profiles for each weekday individually. The profiles were then combined as a representative week.

The SH demand is modelled dynamically, based on the building model described in section 3.1.3. The heat withdrawn from the TBS to activate the CH or the TABS node, is calculated based on mass flow $\dot{m}$, and the temperatures difference between the lower node (T_{SH}) and the corresponding nodes of the building model (T_{CH}) and (T_{TABS}), see Fig. 5.

3.1.3. Model of the building mass

The building model aims to represent the dynamic behaviour of the building and to enable the prediction of realistic indoor conditions, thereby allowing the MPC to ensure occupant thermal comfort. As with the thermal buffer storage, the building is modelled using an RC approach. Building components such as the exterior walls are aggregated into a single thermal mass characterized by an average temperature of all exterior walls. Kuboth et al. modelled a SFH as a single thermal zone using a 5R4C model, in which five thermal resistances and four thermal capacities describe the building dynamics [2]. In their model, the floor is represented by two distinct layers: a thermally activated layer and a surface layer. This allowed for a more accurate depiction of the dynamic thermal behaviour of the floor.

Most of the studied buildings have been dealing with radiator or floor heating systems in which the heat transfer mainly depends on convection. For ceiling heating, the room temperature mainly depends on radiation exchange of the surfaces which relates to the surface temperatures. A 13R5C building model was developed which uses the external walls, internal walls, room air (incl. furniture), rooftop (incl. TABS) and ceiling heating into a separate capacity, see Fig. 5. The subscripts of the resistances (R) represent to which capacities (C) it is connected.

The ceiling of the building was modelled as two layers since the CH and TABS can be activated separately. Also, this is aligned with the modelling approach from Kuboth et al. to represent the dynamics of an activated building element more accurately. The parameters for the capacity and resistances were calculated based on literature values of the used building materials. An overview of the parameters used is given in Table 2 and 3. As suggested by Magni et al. the capacity of the furniture inside the building was estimated and added to the air node to reduce the computation time of the model [4].

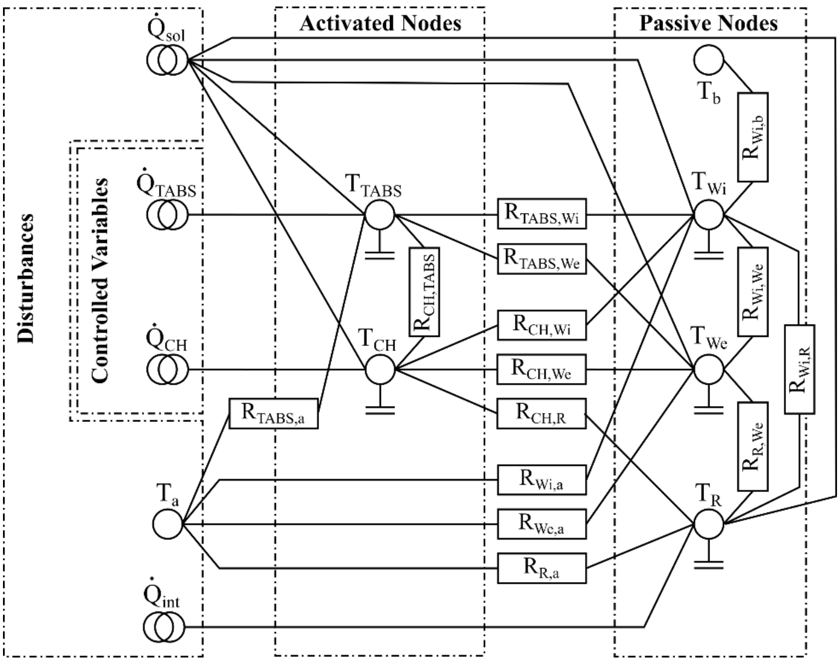

Figure 5. RC-model of the building (a: ambient, Wi: inner wall, We: exterior wall, R: room, b: basement, sol: solar, int: internal)

In comparison to other building RC-models in literature the proposed model has a similar number of capacities but a larger number of resistances. This was done to represent the radiation exchange accurately. Interconnections with smaller influence, such as those between TABS and exterior walls, were also included to account for heat conduction at their junction along the building perimeter. However, it is expected that these resistances could be neglected due to the low specific value of the heat transfer. A more detailed analysis of the building model needs to be done to study which level of detail really is needed to represent the dynamic behavior of a building with ceiling heating.

Table 2. Values for the resistance of the RC-model (Cond: Conduction, Conv: Convection, Rad: Radiation)

Parameter	Value	Transfer Mechanism	Parameter	Value	Transfer Mechanism
$R_{TABS,a}$	47 W/K	Cond & Conv & Rad	$R_{Wi,a}$	23 W/K	Rad
$R_{CH,TABS}$	900 W/K	Cond	$R_{We,a}$	120 W/K	Cond & Conv & Rad
$R_{TABS,Wi}$	200 W/K	Cond	$R_{R,a}$	97 W/K	Cond (window) & Conv & Ventilation
$R_{TABS,We}$	5 W/K	Cond	$R_{Wi,R}$	1000 W/K	Conv & Rad
$R_{CH,Wi}$	300 W/K	Cond & Rad	$R_{Wi,We}$	10 W/K	Rad
$R_{CH,We}$	20 W/K	Cond & Rad	$R_{R,We}$	70 W/K	Conv & Rad
$R_{CH,R}$	300 W/K	Cond & Rad	$R_{Wi,b}$	25 W/K	Cond & Conv

Table 3. Values for the capacities of the RC-model.

Parameter	Value	Description
C_{TABS}	40 kWh/K	concrete core activation layer
C_{CH}	16 kWh/K	ceiling heating layer
C_{Wi}	22 kWh/K	inner walls & slab
C_{We}	16 kWh/K	exterior walls
C_{R}	2 kWh/K	room air and furniture

3.2. Formulation of the optimization problem

The aim of the optimization problem is to minimize an objective function J_{tot} at each time step over the prediction horizon N, see Eq. (2). The objective function consists of two terms: one for the boundary conditions (J_{BC}) and the other for the electric consumption of the ASHP (J_{el}).

$$J_{tot} = \sum_{i=1}^{N}(\omega_1 \cdot J_{BC,i}^2 + \omega_2 \cdot J_{el,i}) \tag{2}$$

J_{el} is calculated based on the developed polynomial approach for the electric power consumption of the ASHP, see Eq. (1). It is important to mention that J_{BC} only occurs if soft constraints are violated and J_{el} whenever the ASHP is operated during the prediction horizon. The weighting parameters $\omega_1 = 1000$ and $\omega_2 = 0.001$ were used. The weighting parameters were defined based on a sensitivity study to reach a good compromise between constraint violation and ASHP operation. The boundaries of the MPC are designed as soft constraints, meaning they are allowed to be violated but lead to certain costs (J_{BC}) during the optimization. As constraint violations are mostly unavoidable in practice, soft constraints in optimization are favorable for robust controller operation.

The model states were defined as T = [$T_{TBS,DHW}$, $T_{TBS,SH}$, T_{TABS}, T_{CH}, T_R, T_{Wi}, T_{We}]. The lower and upper boundary were defined as the temperature vectors [42,20,18,18,21,-inf,-inf] and [60,40,18,18,21,inf,inf] respectively. Since the inner and exterior walls are only passive elements no boundaries were defined for these nodes. The control variables of the MPC were defined as u = [$f_{inv,DHW}$, $f_{inv,SH}$, $\dot{m}_{TABS}$, $\dot{m}_{CH}$] with the units [none, none, kg/s, kg/s]. The lower and upper boundaries were defined as [0,0,0,0] and [0.6, 0.35, 0.3, 0.3] respectively. An equality and inequality constraint were defined in Eq. (3) and (4), to represent that the ASHP can heat up either the DHW or the SH part of the TBS and ensure the validity of the TBS model.

$$f_{inv,DHW} \cdot f_{inv,SH} = 0 \tag{3}$$

$$T_{TBS,DHW} - T_{TBS,SH} \geq 0 \tag{4}$$

3.3. Implementation of the model predictive controller

The MPC is implemented as illustrated in Fig. 6. As described previously, the MPC computes the control schedules (u) for both the operation of the air-source heat pump and the activation of the building's thermal mass. These control signals are forwarded to a second control layer, referred to as the Fall-Back layer, which ensures safe building operation. The Fall-Back layer monitors the measured room and thermal buffer storage temperatures against predefined limits. If any limit is violated, the MPC commands are overridden, and the ASHP and associated pumps and valves are activated or deactivated to restore the system to a feasible operating state as quickly as possible. By this, unwanted under- or overheating situations of the TBS and rooms are prevented or minimized. The altered schedule (u*) is then sent to the system's devices, namely the ASHP and the pumps and valves.

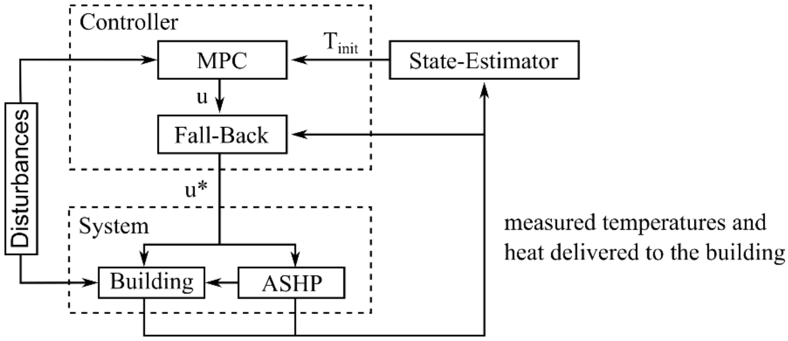

Figure 6. Implementation of the controller architecture in the demonstration building.

The measured system temperatures and heating power delivered to the building are used to execute a state estimator which estimates the unmeasured system states such as the temperature of the CH, inner walls, and exterior walls. The estimated and measured system states (T_{init}) are used to initialize the MPC routine, which is executed continuously in a rolling horizon principle updating the schedule in a regular time step. This helps to ensure robust control since prediction errors (e.g. higher solar gains than anticipated) can be tackled by updating the schedule accordingly.

Since the ASHP is a dynamic system, it requires a comparably frequent update of the control variables. In literature usually a time step of 15 minutes is used [5]. This time step meets the requirement of the ASHP for its minimal run time of 15 minutes. Different prediction horizons were tested to study the time it takes to solve the optimization problem. The calculations were done on a HP EliteBook 840 GS with the CPU Intel Core i5-85250U@1,60 GHz and 16 GB RAM representing a commonly available controller hardware. For the selected step size, a prediction horizon of 16 hours could be solved in less than 15 minutes, providing sufficient dead time before the next MPC execution.

As mentioned before, the demonstration building has a large thermal inertia due to its high thermal mass, insulation standard, and solar gains. Thus, a longer prediction horizon of at least three days is needed to find reasonable schedules for the thermal activation of the demonstration building [6]. To tackle the issue of a longer prediction horizon without increasing the computational resources a hierarchical MPC structure was designed. In Fig. 7 the setup of the hierarchical MPC structure is shown.

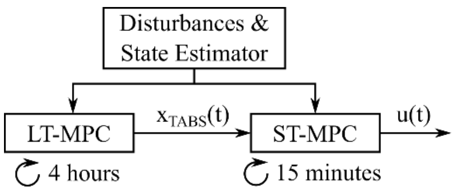

Figure 7. Setup of the hierarchical model predictive controller

A long-term MPC (LT-MPC) calculates the schedule for a prediction horizon of seven days using a step-size of four hours. The LT-MPC updates the schedule of the ASHP every four hours and thus the trajectory of the system's states. The updating frequency was chosen since the online weather forecast is updated every three hours. The predicted trajectory of the TABS node (x_{TABS}) is then used as a goal of the second MPC, the short-term MPC (ST-MPC). The ST-MPC was designed as mentioned before using a prediction horizon of 16 hours and a step-size of 15 minutes. To take the TABS temperatures of the LT-MPC into account, the cost function of the ST-MPC ($J_{tot,ST}$) was extended by a terminal costs term (J_{TABS}), see Eq. (5).

$$J_{tot,ST} = \sum_{i=1}^{N}(\omega_1 \cdot J_{BC,i}^2 + \omega_2 \cdot J_{el,i} + \omega_3 \cdot J_{TABS}) \tag{5}$$

J_{TABS} introduces costs whenever the calculated TABS temperature at the end of the prediction horizon of the ST-MPC does not equal the calculated TABS temperature by the LT-MPC at the same time. By using a high weighting factor ω_3=1000 reaching the same TABS temperature in ST and LT-MPC is prioritized in the cost function. Based on this approach, the ST-MPC has the flexibility to choose the ASHP operation freely within its 16 hours prediction horizon as long as the TABS temperature is reached in the end. Thus, the LT-MPC considers long term weather trends and passes them to the ST-MPC which handles the system dynamics and real time disturbances.

4. Evaluation of the optimized operation

The MPC was implemented in the demonstration building and monitored for one full heating season in real operation. As reference, a previous heating season was monitored using conventional control of the ASHP and no usage of the building mass as a storage capacity. For this study, a period of five days of each operation (non-optimized and optimized) was selected representing similar ambient conditions, see Table 4. While the optimized period shows higher cumulated solar radiation this does not directly reflect higher solar gains as the occupant's usage of shades is unknown.

Table 4. Ambient conditions of selected monitoring periods

	Mean ambient temperature	Maximal ambient temperature	Minimal ambient temperature	Cumulated solar radiation
Non-optimized period	2.6 °C	10.7 °C	-4.2 °C	6443 Wh
Optimized period	2,7 °C	9.9 °C	-5.6 °C	7049 Wh

In Fig. 8 the ASHP operation and measured room and TABS temperatures are shown. For the non-optimized period, the ASHP operation is distributed throughout the whole day while the operation is longer during colder times at night or in the morning. During night-time the heat demand of the building increases due to the higher temperature difference between indoor and outdoor temperatures. In comparison to that, during the optimized period the ASHP operates mainly during the daytime. Occasionally, smaller peaks in the modulation indicate limit violations, during which the Fall-Back layer was activated. For the given case it could be identified that this was mainly due to the bathroom of the building which is heated to a higher temperature due to the occupant's preferences. Due to the simplified building model having only one thermal zone, the bathroom cannot be handled individually by the MPC. A second thermal zone would need to be included in the building model, to predict the behavior of the bathroom as well. However, using only one thermal zone shows that a significant amount of the heat demand can be shifted towards favorable outdoor temperatures.

When comparing the modulation of both periods, the modulation during the non-optimized period is usually around the lower limit of 30%. The modulation during the optimized operation usually is between 40 to 60%. Focusing the operation on favorable outdoor temperatures leads to the fact that the heat demand needs to be covered during a shorter time. Thus, the modulation of the ASHP must be higher. As discussed before, the efficiency of an ASHP depends on its modulation. Exemplary evaluations of the monitoring data showed that the efficiency of the installed ASHP increases significantly when the modulation is low. Thus, in terms of modulation, the operation of the non-optimized period is favorable.

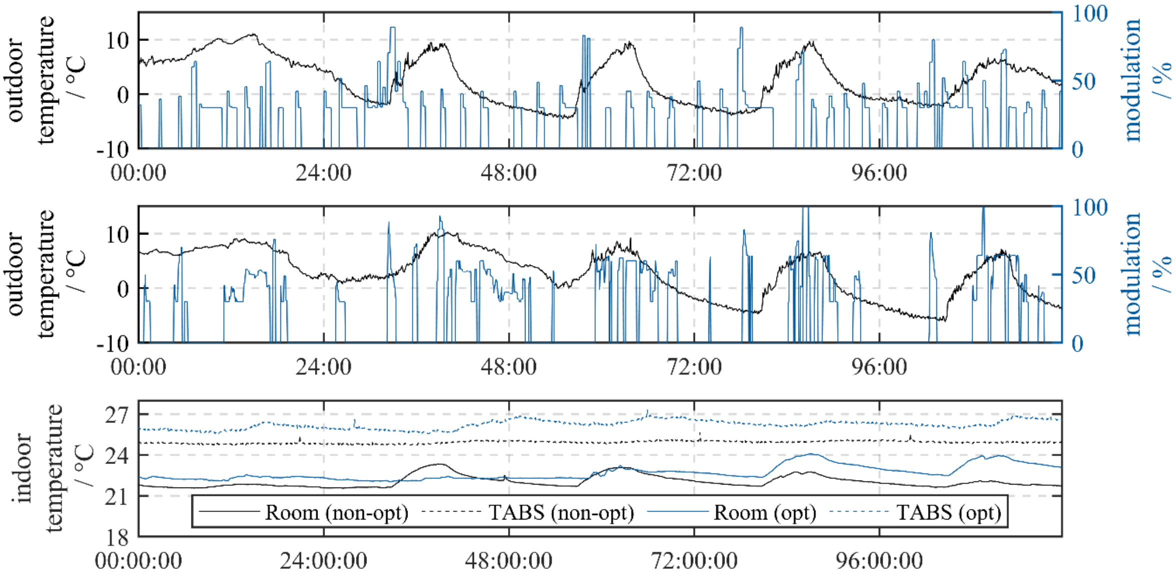

Figure 8. Monitored ASHP operation during an exemplary period during a heating season with conventional control (top), predictive control (middle), and the respective mean room and TABS temperatures of both periods (bottom)

The operative efficiency of the ASHP was evaluated based on the performance factor (PF_{ASHP}), see Eq. (6). The thermal energy measured by the heat meters *ASHP_SH*, *ASHP_DHW*, and the electric energy measured by *ASHP_El* were used for the calculation.

$$PF_{ASHP} = \frac{Q_{ASHP\_SH} + Q_{ASHP\_DHW}}{E_{ASHP\_El}} \tag{6}$$

The resulting PF_{ASHP} increased by 15% from the non-optimized to the optimized period, even though the modulation of the ASHP during the optimized period was not as favorable as during the non-optimized period. Considering the measurement accuracies limits the calculated PF_{ASHP} to a range from 4-27%. This means that even in the worst case, the operative efficiency of the ASHP is increased. The results are listed in Table 5.

Table 5. Measured energy supply and demand inside the demonstration building during an exemplary period of a non-optimized and an optimized period

	Non-optimized period	Optimized period
Q_{ASHP_SH}	139 kWh (±4,2 kWh)	191 kWh (± 5,7 kWh)
Q_{ASHP_DHW}	33 kWh (±1 kWh)	42 kWh (±1.3 kWh)
E_{ASHP_El}	57 kWh (±1.1 kWh)	67 kWh (±1.3 kWh)
PF_{ASHP}	**3.02 (±0,15)**	**3.48 (±0,17)**
Q_{TABS}	0 kWh	140 kWh (±4.2 kWh)
$Q_{TABS,remaining}$	0 kWh	23 kWh
Q_{CH}	136 kWh (±4.1 kWh)	55 kWh (±1.7 kWh)
System efficiency	**100%**	**79%** (±5%)

The lower part of Fig. 8 shows the area-weighted mean of the TABS and the room temperature. In the beginning, the room temperatures of both periods are similar while for the optimized period the temperature increases over time. According to the occupants, the thermal comfort was not violated. However, this needs further investigations, since it can be a result of the activated building mass but also due to differences in solar gains, ventilation behaviour or other external non-controllable effects.

During the optimized period the TABS temperature shows an average offset of 1.3 °C in comparison to the non-optimized period. This indicates that the building mass is on a higher temperature due to its thermal activation. This might lead to higher heat losses of the building lowering its system efficiency and consequently offsetting the benefits of a higher PF_{ASHP}. The system efficiency was defined according to Eq. (7). The heat demand measured by the heat meters for TABS and ceiling heating during the optimized period is divided by the corresponding heat demand of the non-optimized period. This definition was chosen because the building was operated without thermal activation during the non-optimized period, and the SH demand during this time represents the energy required to maintain occupant thermal comfort.

$$\eta_{system} = \frac{Q_{TABS}+Q_{CH}}{Q_{TABS,non-opt}+Q_{CH,non-opt}} * 100\ [\%] \quad (7)$$

By comparing the sum of the measured thermal energy by the heat meters *TABS* and *CH*, a significant increase in heat demand of 59 kWh can be identified. This result needs to be adjusted by the remaining thermal energy stored within the building mass at the end of each period. This can be checked partially based on the measurements of the TABS temperatures. As expected, there was no temperature difference for the non-optimized period since the heat distribution is realized only via the CH. During the optimized period, the area-weighted mean TABS temperature changes by 0.57 K. This value is not affected by measurement uncertainty, since the uncertainty remains constant for small temperature variations and cancels out when temperature differences are considered. Owing to the insulation layers above and below the upper concrete layer, the temperature gradient across the concrete is assumed to be negligible; consequently, uncertainties related to sensor placement are neglected. Based on the heat capacity given in Table 4 and the observed temperature change of 0.57 K, the remaining thermal energy stored in the TABS is estimated at 23 kWh. Subtracting this amount from the heat energy measured by the *TABS* heat meter reduces the difference in thermal energy demand to 36 kWh, which remains higher than expected. This results in a system efficiency of 79% for the evaluated periods. Due to the loss in system efficiency, the electric consumption of the ASHP is higher for the optimized period.

As the TABS constitutes only a portion of the overall building mass, additional energy may remain stored in other building components at the end of the optimized period, potentially further reducing this discrepancy. Also, the comparability of both periods was only based on ambient conditions. Further influences such as the occupant's ventilation behavior and internal gains of the building can be different. Thus, the calculated results are preliminary and must be seen as a first comparison. Besides the higher heat losses due to the building mass activation the predictive control of the building may make better usage of the solar gains by cooling the building mass further down compared to the conventional controller. This yields the potential that the building operation becomes more efficient, and heat demand is decreased. Thus, more periods or ideally the complete heating period should be evaluated, e.g. based on climate adjustment methods. A more detailed comparison of both heating periods must be made to analyze and understand the impacts and effectiveness of the predictive controller in detail.

5. Conclusion and Outlook

Using the building mass as a thermal storage capacity yields a high potential for optimizing an ASHP by shifting the operation to favorable outdoor temperatures. This can be realized by using advanced predictive control algorithms, such as MPC. When designing and implementing an MPC for ASHPs several aspects need to be considered: non-linear ASHP behavior, high thermal inertia of the building mass, and robust control.

An MPC was designed and implemented in a demonstration building. The building model was aligned with approaches from literature and extended to represent the dynamic behavior of the ceiling heating system of the demonstration building. The presented approach serves as a first approach. A more detailed study of the simplified models should be done in future to understand which level of detail is needed. The heat pump model was designed based on measurement data from the data sheet of the installed ASHP. Since there was no information about the inverter influence on the efficiency of the ASHP, this effect was covered using an adjusted cost function aligned with the suggestions by literature [3]. To reach reasonable computational times for calculating the schedule of ASHP and building activation, a hierarchical approach consisting of a LT-MPC and a ST-MPC was implemented. Following this approach a prediction horizon of seven days could be realized while considering the non-linearities of the ASHP and having a resolution of the schedule of 15 minutes.

The building has been monitored during two heating periods using the conventional controller and the developed MPC to operate the heating system and the ASHP. Based on the measurement data an efficiency increase between 4-27% was achieved for an exemplary period of the non-optimized and the optimized heating season. For the chosen period, this positive effect was negated by a lower system efficiency leading to higher electricity consumption of the ASHP. The results may change when considering a complete heating season, which will be done in the next step.

Ultimately, a similar comparison using a conventionally controlled heating season and an optimized heating season will be made also for a renovated building. This brings insights into the potential of using the building mass as storage capacity with a lower insulation standard and thus higher storage losses. Also, instead of using CCA or ceiling heating the thermal activation of floor heating systems can be of interest since this heat distribution system represents most installed residential heating systems.

Acknowledgements

This study was supported by the Federal Ministry of Economics and Energy on the basis of a decision by the German Bundestag within the research project “optLWP” (03EN1054A).

References

[1] Thür A, Schett B, Leu F. PV driven Air Heat Pump using Overheating Effects as Thermal Battery in Single Family Houses. In: International Solar Energie Society, editor. EuroSun 2022 Proceedings; 2022.
[2] Kuboth S, Heberle F, König-Haagen A, Brüggemann D. Economic model predictive control of combined thermal and electric residential building energy systems. Applied Energy 2019;240:372–85. https://doi.org/10.1016/j.apenergy.2019.01.097.
[3] Verhelst C, Logist F, van Impe J, Helsen L. Study of the optimal control problem formulation for modulating air-to-water heat pumps connected to a residential floor heating system. Energy and Buildings 2012;45:43–53. https://doi.org/10.1016/j.enbuild.2011.10.015.
[4] Magni M, Ochs F, Streicher W. Comprehensive analysis of the influence of different building modelling approaches on the results and computational time using a cross-compared model as a reference. Energy and Buildings 2022;259:111859. https://doi.org/10.1016/j.enbuild.2022.111859.
[5] Hilliard T, Kavgic M, Swan L. Model predictive control for commercial buildings: trends and opportunities. Advances in Building Energy Research 2016;10(2):172–90. https://doi.org/10.1080/17512549.2015.1079240.
[6] D’Ettorre F, Conti P, Schito E, Testi D. Model predictive control of a hybrid heat pump system and impact of the prediction horizon on cost-saving potential and optimal storage capacity. Applied Thermal Engineering 2019;148:524–35. https://doi.org/10.1016/j.applthermaleng.2018.11.063.
[7] Langner F, Frahm M, Wang W, Matthes J, Hagenmeyer V. Hierarchical-stochastic model predictive control for a grid-interactive multi-zone residential building with distributed energy resources. Journal of Building Engineering 2024;89:109401. https://doi.org/10.1016/j.jobe.2024.109401.
[8] Sinnesbichler H, Kersken M. Thermische Energiespeicher: Windheizung 2.0: Entwicklung von zentralen Hochtemperatur- und Bauteil-Langzeit-Speichern für Windheizung 2.0 Wohngebäude; 2023.
[9] Schmitt D, Reum T, Summ T, Trinkl C, Schrag T. Investigation of the Flexibility Potential by Decoupling Building Mass and Room Temperature. Int Sustain Ener Conf Proc 2024;1. https://doi.org/10.52825/isec.v1i.1165.
[10] Drgoňa J, Arroyo J, Cupeiro Figueroa I, Blum D, Arendt K, Kim D et al. All you need to know about model predictive control for buildings. Annual Reviews in Control 2020;50:190–232. https://doi.org/10.1016/j.arcontrol.2020.09.001.
[11] The MathWorks Inc. Model Predictive Control Toolbox (Version 2024b).
[12] DIN-Normenausschuss Kältetechnik. Luftkonditionierer, Flüssigkeitskühlsätze und Wärmepumpen für die Raumheizung und -kühlung sowie Prozesskühler mit elektrisch angetriebenen Verdichtern: Teil 2: Prüfbedingungen(DIN EN 14511); 2024-03-00.
[13] The MathWorks Inc. Curve Fitting Toolbox (Version 2024b).